Transient Liquid Crystal Thermometry of Microfabricated PCR Vessel Arrays

Ajit M. Chaudhari, Timothy M. Woudenberg, Michael Albin, and Kenneth E. Goodson

***Abstract*— Polymerase chain reaction (PCR) using micromachined structures promises improved temperature uniformity and cycling time together with decreased reagent and sample volumes. Thermal design of these structures will benefit from measurements of the temperature distribution in the reacting liquid. We report measurements of temperature uniformity and time constant in a microfabricated 18-vessel array using encapsulated liquid crystals suspended in the liquid. Separate sets of crystals are used to image temporal and spatial temperature variations near the processing thresholds of 55°C and 95°C with a resolution of 0.1°C. While the thermometry technique developed here is particularly useful for characterizing microfabricated PCR systems, it can also aid with the thermal design of a broad variety of microfluidic devices. [330]**

***Index Terms*— Design, liquid crystals, microfabrication, microfluidic, polymerase chain reaction, thermometry.**

I. Introduction

In the last decade, the polymerase chain reaction (PCR) has become an important tool in biomedical research for the replication of DNA. Recent advances include real-time detection of PCR, which allows *in situ* optical interrogation of the amplification process and offers the potential for greater control and reproducibility [1]. Another major advancement, which is the subject of current research, is the realization of PCR in microfabricated vessel arrays [2]–[5]. While this approach promises improvements in the time and sample volumes required for PCR, it also poses challenges for thermal design that have not been addressed. This manuscript identifies these challenges and presents solutions in the areas of thermal modeling and thermometry.

The realization of miniature PCR vessels using microfabrication technology offers several advantages compared to conventional PCR techniques in use today. Aside from the significant cost benefit which results from the lower reagent use, microfabricated arrays offer the possibility of major improvements in temperature uniformity and thermal time constant. Because of the smaller heat capacity of the vessel and the reagents, the amount of power necessary to perform high-speed cycling is orders of magnitude less than for conventional PCR systems based on multiple vials. Because the microfabricated array can occupy a smaller volume, the temperature nonuniformity that results from nonuniform heating of the chip or nonuniform thermal contact resistance between chip and heater can be significantly less, and the speed at which these nonuniformities decay is dramatically faster. The high rate at which samples can be cycled is also an important benefit of microfabricated PCR vessel arrays. This results in part from the smaller sample size, which allows faster changes in temperature for a given power and strongly diminishes the time required for those temperature changes to propagate through the sample. The increased cycling rate results also from the use of silicon rather than plastic to contain the samples. The plastic tubes in conventional PCR systems contribute a large thermal resistance, which strongly impedes heating and cooling of the samples. The tube has a thermal conductivity that is significantly less than the water-based contents and is nearly three orders of magnitude less than that of silicon.

Although microfabricated PCR vessel arrays offer the possibility of improved temperature uniformity and reduced time constant, these can only be achieved through careful thermal design and validation. The transient temperature distribution in the array depends strongly on the placement of the heat source on the vessel array and the thermal characteristics of the mounting and packaging for the microfabricated structure. The importance of temperature uniformity and thermal design of microfabricated PCR systems is demonstrated by preliminary data taken as part of the current study. A standard dilution series of β-actin is performed using three different sets of temporal temperature plateaus (Fig. 1). For the optimal set of temperature plateaus [Fig. 1(b)], the agreement of the fluorescence data taken for the inner and outer vessels demonstrates the best consistency within the array. The temperature nonuniformity of the device is estimated to be <0.5°C during the plateaus. When the plateau heater temperature is below the optimum value [Fig. 1(a)], the warmer of the pairs perform better as indicated by a higher final signal or earlier initial rise. When set above optimum [Fig. 1(c)], the colder of the pairs performs better. When close to the optimum setting, the differences are minimal. These data show that differences in the average vessel temperatures (<0.5°C) are much less important when the temperature plateaus are near the optimum values. However, if there is any departure from the optimum cycling history, much smaller temperature nonuniformity can yield substantial errors. Without careful design and validation to assure temperature uniformity and the elimination of these

Manuscript received February 13, 1998; revised August 29, 1998. This work was supported under a grant from the National Institute of Standards and Technology with additional support from the Advanced Technology Program for DNA Diagnostics, Perkin Elmer Applied Biosystems, EG&G IC Sensors, NSF CAREER Program, and ONR Young Investigator Program. EG&G IC Sensors also provided technical input. Subject Editor, K. J. Gabriel.

A. M. Chaudhari and K. E. Goodson are with the Mechanical Engineering Department, Stanford University, Stanford, CA 94305 USA.

T. M. Woudenberg and M. Albin are with PE Applied Biosystems, Foster City, CA 94404 USA.

Publisher Item Identifier S 1057-7157(98)09014-3.

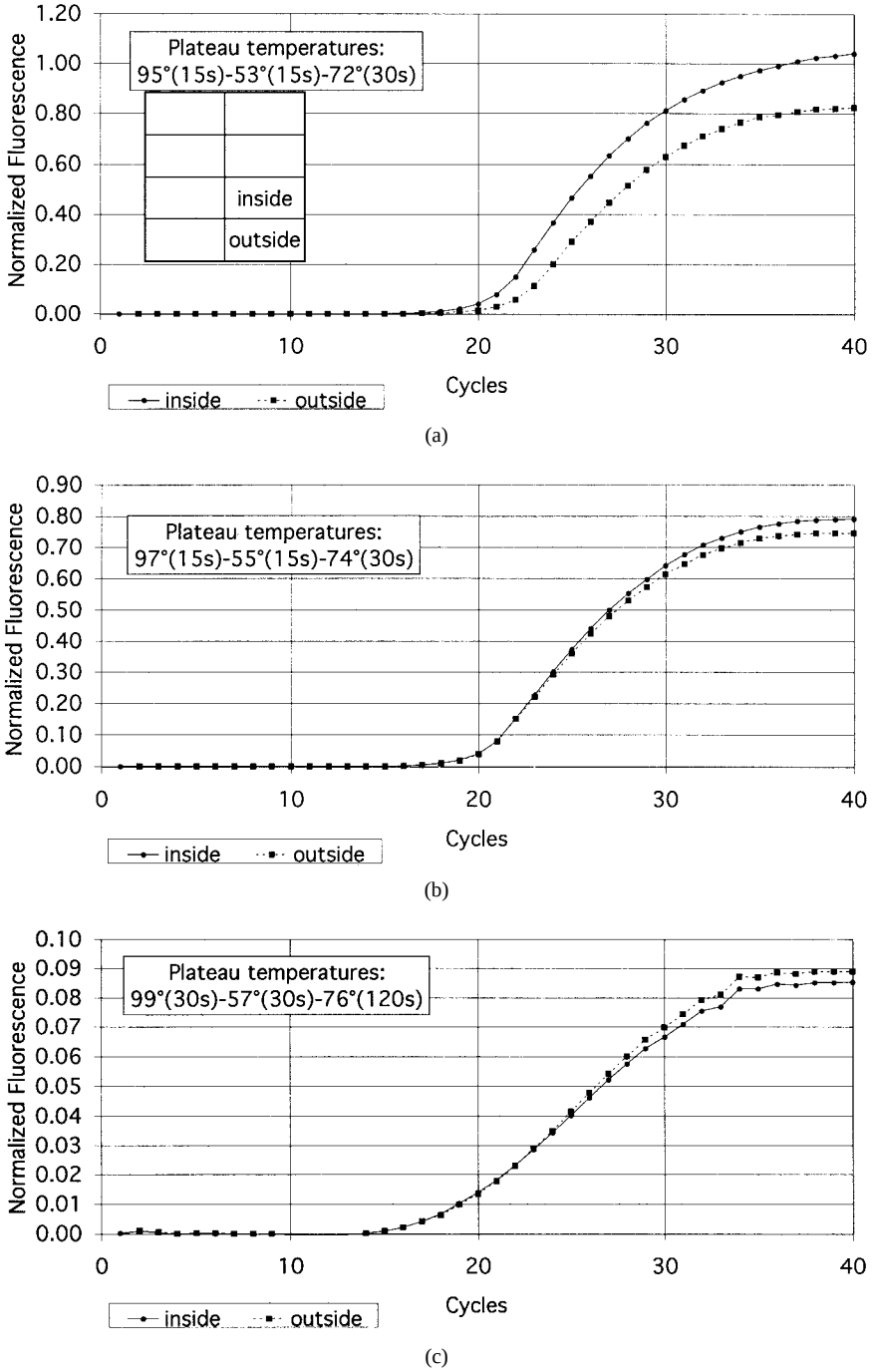

Fig. 1. Cycle plots for a standard dilution of human DNA. Initial concentration of DNA molecules is 6000 copies/5 μl well. The vessel array used in this set of experiments was similar to that shown in Fig. 2 except that each vessel had a capacity of 5 μl, allowing only eight vessels to fit on the chip. The assay is for the β-actin sequence. The plots show the results for three different temperature cycles. The individual samples are arranged on the chip such that one sample of the replicate pair is on the outside edge and one is on the inside. A top view of the 5-μl vessel array showing the locations of the two samples is inset in each plot. The outer ones (slightly colder vessels) are plotted with solid lines, while the inner ones (slightly hotter vessels) are plotted with dotted lines. (a) The plots show that when the cycling temperatures are too low, the hotter inner vessel performs better, as determined by an earlier initial rise or higher final signal. (c) When the cycling temperatures are too high, the colder outer vessel performs better.

differences in replication, the reliability and repeatability of PCR across the different vessels of the array are compromised.

Thermal simulations are required to develop a vessel geometry and packaging that improve temperature uniformity, and thermometry is required to demonstrate that it has been achieved. The problem of thermometry is particularly challenging, since there is no technique that is ideally suited for microfabricated PCR systems. Although thermocouples and electrical-resistance thermometers can be attached to the silicon die or inserted in the vessels, they can dramatically change the temperature distribution in the microfabricated array. While this problem can be overcome by patterning microscopic thermocouple junctions and electrical-resistance or diode thermometers directly on the silicon die, these small

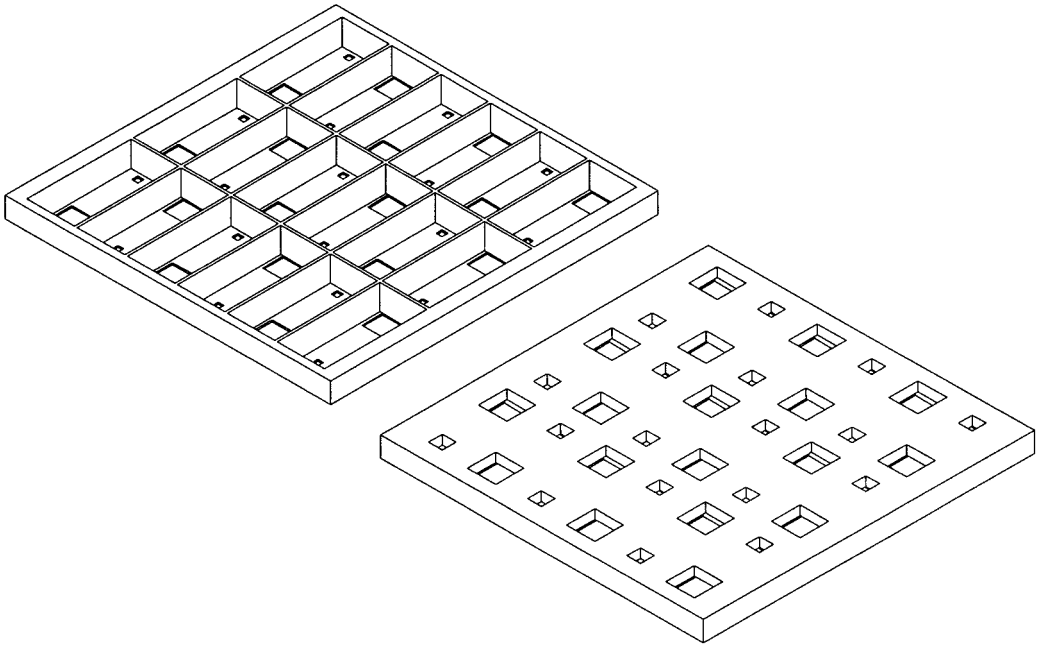

Fig. 2. Schematic of a micromachined silicon reaction vessel array for PCR. The top side (left) is sealed with 0.5-mm-thick Pyrex glass (not shown) through which TLC thermometry is performed. The working fluid is loaded through the square ports on the bottom side (right). The silicon component of the array (shown) has overall dimensions 11.0 mm × 11.2 mm × 0.7 mm.

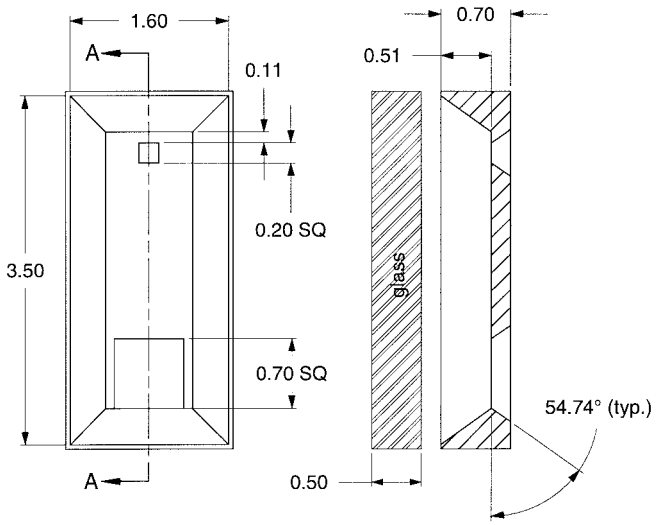

Fig. 3. Schematic of a single vessel showing the dimensions. (a) The top view shows the sizes of the loading and vent holes. The Pyrex glass plate shown in (b) is bonded to the silicon chip to seal the vessel on its top side. All dimensions are in millimeters.

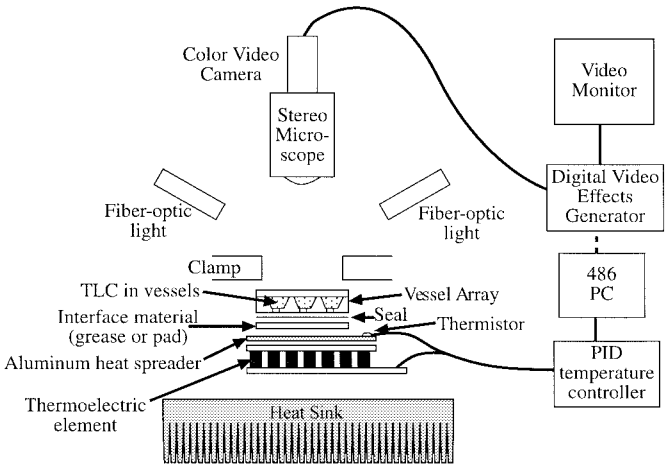

Fig. 4. Experimental apparatus for temperature mapping. The image of the TLC-filled vessels is passed to the digital effects generator, which adds an inset with time and temperature from the PC screen. The PID controller converts the thermistor resistance value to temperature.

thermometers yield temperature data only at a few discrete points or lines within the system. Moreover, the use of aluminum lines on the inner walls of the vessels is not viable as metals inhibit the reaction. Infrared thermometry will only provide information about the surface temperature of the infrared-absorbing glass cover, which can differ substantially from that of the reagents.

This work proposes a technique for measuring temperature fields in microfabricated PCR vessel arrays using thermochromic liquid crystals (TLC's). TLC's are a class of organic chemicals, usually cholesterol derivatives, with optical properties that are strongly sensitive to temperature within ranges specific to their chemical composition [6], [7]. Within the sensitivity range of a given TLC, the wavelength-dependent reflectivity varies strongly with temperature and induces a strong temperature dependence of the apparent color. The color can be quantified through the hue, which can be calibrated. Although these crystals are most commonly used for thermometry of dry surfaces, they can be suspended in liquids when encapsulated by a protective polymer. This work describes measurements in which the crystals are loaded into the liquid in microfabricated PCR vessel arrays and used to observe temporal and spatial variations in temperature. After inserting TLC's in each vessel, the temperature of

the vessels is cycled in the same way as it would be for PCR, and the hue changes are recorded. The data resulting from this study confirm that the studied microfabricated PCR system can shorten cycling times and provide adequate temperature uniformity. While the thermometry technique developed here is particularly useful for PCR vessel arrays, it offers benefits for thermometry and flow visualization in a broad variety of microfabricated fluidic systems including microchannel heat exchangers, thermally actuated microvalves, and electrophoresis-driven pumps.

Section II describes the experimental apparatus including the thermochromic liquid crystal system and its calibration. Section II also describes the experimental procedure, the determination of the time constant, and the results of finite-element modeling. Section III discusses the results of the experiments and their implications for the thermal design of the microfabricated PCR system. Section IV provides concluding remarks of general relevance for a microfabricated PCR.

II. Experimental Apparatus and Procedure

The main components of the experimental apparatus are the microfabricated PCR vessel array and the thermochromic liquid crystals used for thermometry. This section also describes a method for *in situ* calibration of the liquid crystals as well as the methods for clamping and controlling the temperature of the vessel array. The temperature difference between the TLC's within the vessels and the heat source is used to determine the time constant. This approach uses both closed-form analytical and finite-difference thermal conduction calculations.

A. Micromachined Silicon Vessel Array

The arrays used in these experiments, shown in Fig. 2, contain 18 vessels in a 3×6 array configuration. Each vessel is equipped with a 0.7×0.7-mm hole for manually filling the vessel with liquid as well as a smaller vent hole to allow air to escape during filling (see Fig. 3). Each vessel has a volume of 2 μl. To fabricate the vessel array, a 0.70-mm-thick silicon wafer is anistropically etched to yield 0.5-mm-deep wells after which the fill and vent holes are etched from the opposite side. A 4000-Å layer of thermal oxide is then grown on the etched surfaces of the vessels. The final step in processing is to anodically bond 0.5-mm-thick Pyrex glass to create a ceiling for the vessels with optical access. Once the liquid has been added to the vessel array, an acrylic-based adhesive tape that is compatible with PCR chemistry is used to seal the vessels [2].

B. Mounting and Temperature Control

The vessel stage consists of a thermoelectric module, heat sink, and additional aluminum plate to provide even heating. A bead thermistor is glued to the top of this plate to measure temperature. Both the thermoelectric module and the thermistor are connected to a temperature controller for active proportional-integral-derivative (PID) control of the plate temperature. This temperature controller is connected to a PC and operated using a custom-designed interface (Fig. 4). In addition to the acrylic-based clear adhesive tape to seal the vessel array, other interface materials are also placed between the array and the thermoelectric module to reduce the resistance to heat flow. The materials used in these experiments are thermally conductive silicone grease and a thermally conductive plastic pad. Two different plastic clamps hold down the silicon vessel array, with contact surfaces which engage the top four edges of the vessel array (see Fig. 5). The smaller clamp has a total contact area of approximately 5.6 mm^2 while the larger clamp has a contact area of approximately 18.6 mm^2. While the clamp with the larger contact area is simpler to mount, it augments temperature nonuniformities since the clamps are effectively at room temperature. Due to the variability of the mounting procedure for the smaller clamp, however, the contact area for that clamp could vary by approximately $\pm 50\%$. To provide an adequate clamping force, four screws with springs push down on the corners of the clamp. An important goal of the present work is to determine the impact of the simpler clamping method on the temperature uniformity in the vessel array and to determine if it will yield appreciable degradation in the rate of false positive measurements using PCR.

C. Thermochromic Liquid Crystals

Thermochromic liquid crystals (TLC's) are a class of organic cholesteric molecules which exhibit an intermediary phase between the solid and liquid states. While in this phase, the molecules have a reflectivity that is strongly wavelength dependent. The wavelength of maximum reflectivity decreases with increasing temperature within a range specific to the chemical composition, which can be customized. After they have been encapsulated by a nonreactive polymer, beads of TLC's can serve as long-lasting coatings for surface thermometry or as neutrally buoyant temperature and/or velocity markers in a fluid [6], [7], [9]–[11].

Most work with TLC's has used them in solid surface coatings. Accurate visualization of surface temperatures is achieved through the use of uniform coating thickness above a black base paint as well as uniform lighting intensity. By digitally acquiring and analyzing these images, it is possible to determine the temperature distribution at the surface and, given an independent measurement of the heat flux, the local value of the heat transfer coefficient [8]. Painting the surfaces inside a microfluidic device before final assembly is not feasible because TLC's cannot withstand the high temperatures or ultrasonic vibrations necessary to bond the glass to the silicon. Moreover, it is important to be aware of any temperature nonuniformity between the center and walls of the vessel, which cannot be determined from the surface temperature.

Some researchers have used neutrally buoyant encapsulated TLC's in liquids to visualize temperature gradients and fluid motion. These experiments have all focused on natural convection in experimental vessels having volumes larger than one cubic foot [10], [11]. In these experiments, TLC-filled liquid was placed in clear plastic box-shaped vessels with heating on one vertical wall. In this way, the TLC's can be viewed against a flat black background by focusing the light on a plane of liquid oriented normal to the viewing direction. When using

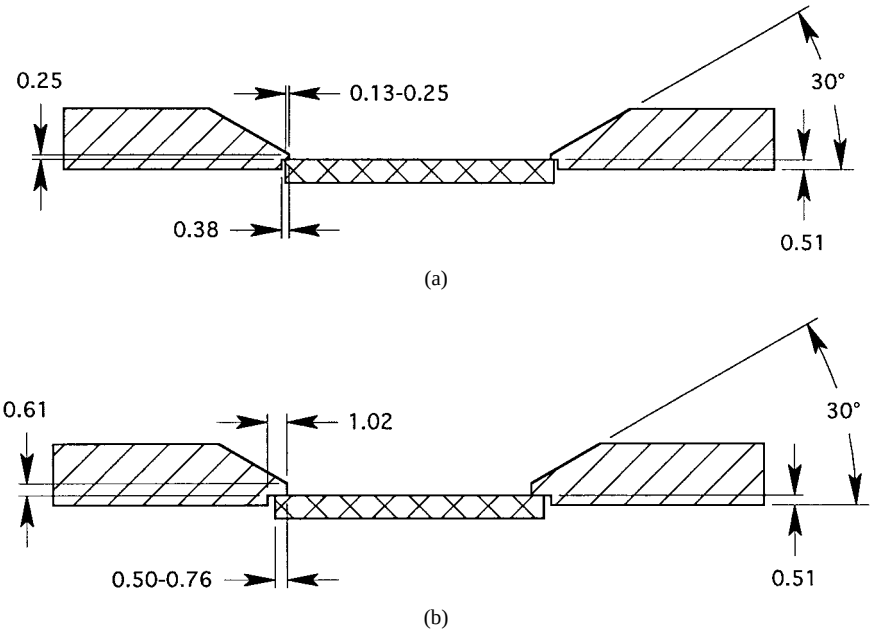

Fig. 5. (a) Section views of the small contact-area clamp and (b) large contact-area clamp. All dimensions are in millimeters. The increased contact surface of the large clamp and extra thickness near the contact surfaces allow larger heat flux to the clamp.

TLC *in situ*, however, a flat black background often cannot be readily imposed, therefore, much more reflected background light is present. As a result, TLC capsule concentration cannot be increased to increase color saturation, as background light reflections make the capsules appear white. The concentrations that provide optimum color response do not make a continuous color map, but rather a constellation of points of color. Because of these problems, image analysis by computer is impractical. However, once calibrated *in situ*, TLC's can provide quantitative thermometry data for the entire temperature distribution at once as represented by a hue map.

In the present work, two formulations of crystals are employed for suspension in liquid in the microfabricated PCR vessel arrays (Hallcrest, Chicago, IL). The first formulation has an operating temperature range of approximately 1°C centered about 55°C and is used to study the temperature distribution during the PCR annealing step. The second formulation has an operating temperature range of approximately 2°C centered about 95°C and is used to study the temperature distribution during the denaturation step of the PCR process. The lower temperature liquid crystals are slightly denser than water and sink to the bottom when loaded in the vessels. The higher temperature crystals, on the other hand, are slightly less dense than water and float up at the ceiling of the vessels. While this complicates comparison of the data obtained at the two temperatures, these differences in density allow the temperature uniformity to be gauged independently at the floor and the ceiling of the vessels.

D. Illumination and Imaging

The illumination and videotaping methods are critical to timing the color changes of the TLC's and to achieving reproducible results. Two optical fibers oriented at 30° from horizontal on opposite sides of the stage illuminate the vessel array. The use of two fibers reduces the importance of shadows, while the angle provides the best signal-to-background ratio. Preliminary experiments determine that the use of polarized light and a polarizing filter do not improve the signal-to-noise ratio significantly, such that these are not warranted in the experimental system. A stereo microscope achieves the necessary magnification. An instrument-grade color video camera captures the images on video. Another video camera and a digital video effects generator provide a real-time inset (picture-in-picture) with time and temperature to the image of the reaction vessels. In this manner, it is possible to examine the videotape in slow motion and determine the temperature lag while ramping up the heater temperature. Images are captured from the video for temperature uniformity analysis. Using this equipment configuration, it is possible to determine the temperature uniformity between the vessels (intervessel) and within vessels (intravessel) for both transient and steady-state cases.

E. Calibration and Uncertainty

Since the images obtained from any TLC experiment depend sensitively on the illumination technique and the properties of materials throughout the optical path, it is essential to recreate the experiment as closely as possible during the calibration procedure. For this reason, calibration is performed on the TLC's in the microfabricated vessel arrays under nearly steady-state conditions, during which the array can be well approximated as isothermal. The temperature of the vessels during calibration is measured independently using a ceramic bead thermistor of a diameter of 0.25 mm and length of 1 mm, which is inserted directly into the liquid in one of the vessels near the center of the array. The impact of heat losses along the leads on the temperature reported by the thermistor has been determined to be negligible using a fin analysis. During

calibration, images of the PCR vessel array are captured for 15 temperatures within the active range of each of the two formulations of crystals. Images from experiments can then be compared to these charts to determine the experimental sample temperature.

In the absence of a computer-based data interpretation system for measurements of hue, which is not provided in the present work, the uncertainty in measuring temperature using TLC is governed by the human ability to distinguish between shades of color corresponding to adjacent temperature steps. At the upper parts of the range, i.e., in the purple region, the resolution error of the TLC becomes the dominant factor, as the color may appear unchanged over 0.5°C. To avoid this region, measurements are taken when in the blue region or below, where the color response resolution is 0.1°C or better. Over the range within which the TLC were used, the uncertainty is approximately ±0.1°C. Another significant source of error results from the contribution of the thermistor used for measuring liquid vessel temperature during the calibration. The thermistor uncertainty is 0.05°C for measurements of temperature changes. Together with the other uncertainty components, this yields an overall uncertainty of ±0.11°C for the measurement of temperature differences in the microfabricated PCR vessel array. The technique used for measuring the time constant requires only the measurement of the temperature difference between the heater and sample. The uncertainty in calculating the time constant is influenced by the ±0.11°C uncertainty due to temperature measurement, which, given the ramping rate for the temperature, results in a time constant uncertainty of less than ±0.13 s.

F. Determination of the Thermal Time Constant

For transient measurements of the vessel array time constant, the temperature lag between the heater and silicon vessel array is measured as a function of the ramp rate. If it is assumed that the vessel array behaves approximately as a lumped thermal capacitor, then the equation governing their temperature is given by

$$C\frac{dT_v}{dt} = \frac{T_h - T_v}{R_1} - \frac{T_v - T_\infty}{R_2} \tag{1}$$

where T_∞ is ambient temperature, T_v is the vessel array temperature, and T_h is the heater temperature. The lumped thermal capacitance of the vessel array is C, and R_1 and R_2 are the thermal resistances between the heater and vessel array and ambient, respectively. By assuming that the measurements are being taken after subjecting the heater temperature to a constant ramping rate β for a time much longer than the time constant τ, the heater-vessel temperature difference $\theta = T_h - T_v$ is given by

$$\theta = \theta_0 + \tau\beta \tag{2}$$

where θ_0 is the steady-state temperature difference between the heater and vessel. Therefore, at any time much longer than the time constant, the measured temperature difference will be a function of the ramp rate. The imaging system described in Section II-D is used to capture data for θ at different ramp rates. Once θ is plotted as a function of β, the time constant is given by the slope of the linear regression line if θ_0 is assumed to be independent of the time constant (2).

For completeness here, it is useful to note the theoretical relationship between the parameters in (2) and the resistances in (1). The heater-vessel temperature difference is

$$\theta_0 = \frac{R_1}{R_1 + R_2}(T_h - T_\infty) \tag{3}$$

and can be understood as the difference that would be achieved under steady conditions if ramping were terminated. The time constant is

$$\tau = \frac{R_1 R_2^2 C}{(R_1 + R_2)^2} \tag{4}$$

and characterizes the lumped-capacitor response of the vessel array to changes in heater or ambient temperature (e.g., [12]).

The model developed in this subsection relies on several assumptions. First, it is assumed that temperature variations in the vessel array are small compared to those between the array and both the heater and the ambient. This is strictly valid when the thermal resistances within the silicon and liquid regions in the array are small compared to the resistance between the silicon and the ambient, which is governed by conduction through the Pyrex ceiling, and the resistance between the silicon and the heating element, which is governed by conduction through the interface material. While this criterion is well satisfied for the silicon regions due to the large thermal conductivity of this material, the thermal resistance of the liquid cannot be neglected. To determine the impact of the liquid resistance on the validity of (2), we perform here a transient finite-element simulation of heat diffusion into a single vessel. The silicon walls of the vessel are modeled as isothermal boundaries, with an enforced temperature boundary condition which increases linearly at $\beta = 2$°C/s from ambient to 33°C above ambient. At the beginning of this time step, the water and silicon have a uniform temperature, so θ_0 is zero. Heat transfer within the vessel is modeled as conduction through water only because free convection is determined to be negligible in this case using experimental correlations [13, p. 542]. In addition, the influence of TLC particles is considered negligible because they comprise less than 2% of the solution by volume.

Fig. 6 shows the maximum and minimum temperatures of the vessel model. The maximum temperature occurs at the silicon boundary, while the minimum occurs at the center of the glass boundary. After the initial increase of the temperature difference in the first 3.0 s, the plot shows that the difference between maximum and minimum temperatures increases only 0.02°C over the 13.5-s duration of the simulation. This discrepancy results from the fact that the temperature difference is also a weak function of the difference between the heater and ambient air. However, this effect is so small that it is insignificant in comparison to the resolution error of the liquid crystals, which is ±0.11°C and discussed in Section II-E. Therefore, the method of measuring effective time constant using (2) is deemed appropriate. As the temperature of the heater rises, the entire temperature distribution is essentially quasi-static, so (2) will give a reasonable estimate of the time

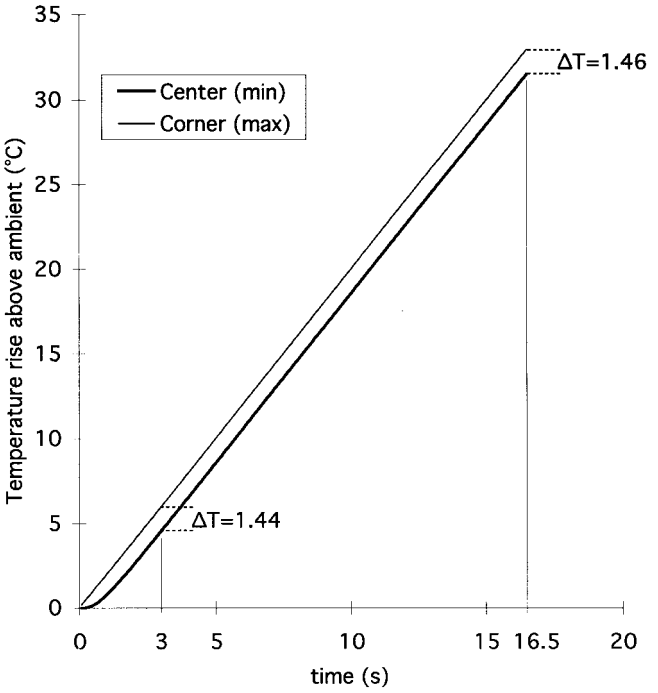

Fig. 6. Predictions from the transient 3-D finite-element simulation of a single vessel subjecting to a transient, positive, temperature ramp at the rate of 2°C/s. The thin line denotes the maximum temperature which occurs at the silicon wall, where a linear rising temperature boundary condition is enforced. The thick line denotes the minimum temperature, which occurs at the center of the glass ceiling, where a convection boundary condition is enforced. After the initial growth, the difference remains essentially constant throughout the simulation from $t = 3$ s to $t = 16.5$ s.

constant (i.e., the most conservative one) if the minimum temperature is chosen. Effectively, the finite-element model shows that it is valid to lump the "floors" of the silicon vessels into the resistance R_1 and predict the time constant on the basis that the water contains most of the capacitance of the system.

III. Results and Discussion

The purpose of this section is to illustrate the usefulness of the suspended encapsulated liquid crystals for thermal diagnostics through results for the microfabricated PCR system described in Sections II-A and B. This section also aims to provide specific information for the example system about the impact of the materials and geometry used for mounting the silicon die on the temperature uniformity and the time constant. Table I summarizes the results for the experiments. The experiments show that the PCR vessel arrays can provide the temperature uniformity and temporal response required for improved PCR if care is taken with the clamp configuration and the choice of interface material. The clamping technique and choice of interface material are both shown to strongly influence the intervessel and intravessel temperature uniformities.

A. Measurements of Intervessel Temperature Uniformity

Experiments are performed while varying both the clamp contact area and the interface material between the silicon chip and the aluminum plate. The interface material provides a nearly uniform thermal contact resistance between the temperature controller and the silicon die. The choice of clamp and interface material strongly affects the temperature uniformity. Fig. 7 shows that at the threshold temperature of 95°C, the clamp with the smaller contact area, 5.6 mm^2, yields temperature variation among the vessels of less than 0.3°C. In contrast, the clamp with larger contact area, 18.6 mm^2, yields variations that exceed 0.6°C near the same threshold temperature. Fig. 7 also shows that the shapes of the temperature distributions are substantially different, with the smaller contact area clamp yielding a more radially symmetric distribution. This suggests that heat losses from the side walls through paths other than the clamp, such as natural convection and radiation from the side walls and conduction into the aluminum heat sink, are dominant for the clamp with the smaller area, while losses through the clamp are significant for the case of the larger contact area. This hypothesis is consistent with the fact that the temperature controller must be maintained at a higher temperature for the case of the clamp with the larger contact area to achieve a similar spatially averaged temperature rise in the vessel array. The larger contact area reduces the thermal resistance between the die and the ambient temperature through its impact on the path through the clamp, which necessitates a higher temperature setting at the controller for maintaining the die temperature near 95°C. This explanation is also consistent with the observation that the clamp with the larger contact area becomes much warmer during the experiment than the clamp with the smaller contact area.

TABLE I
Summary of Results for Experiments Involving Variation of the Interface Material and the Clamp

Clamp	Interface Material	Non-Uniformity at 55 °C	Non-Uniformity at 95 °C	Time Constant (±0.07 s)
Large contact area (18.6 mm^2)	Acrylic sealing tape only	0.2 °C	0.3 °C	0.23 s
	Uneven greasing	0.3	0.3	0.14
	Even greasing	0.3	0.3	0.21
	Thermally conductive pad	0.3	0.6	0.77
Small contact area (5.6 mm^2)	Thermally conductive pad	0.2	0.4	0.69

In all cases, the clear acrylic tape of thickness near 0.05 mm is used to seal the vessels. In two of the trials, no other interface material is used, while in others a thermally conductive pad or silicone grease is used. The clamping technique with larger contact area is used in these experiments. Fig. 8 shows that the cases of no additional interface material and of greasing allow for temperature uniformity of 0.3°C or better. When using the thermally conductive pad, however, the intervessel temperature nonuniformity is as high as 0.6°C. Since the interface materials add varying contributions to the thermal resistance between the temperature controller and the silicon, they affect the offset of the vessel temperature from the heater temperature. Using tape only results in the smallest offset, between 1.4°C and 1.6°C at the threshold temperature of 95°C, while the thermally conductive pad results in the largest offset, between 2.2°C and 2.8°C.

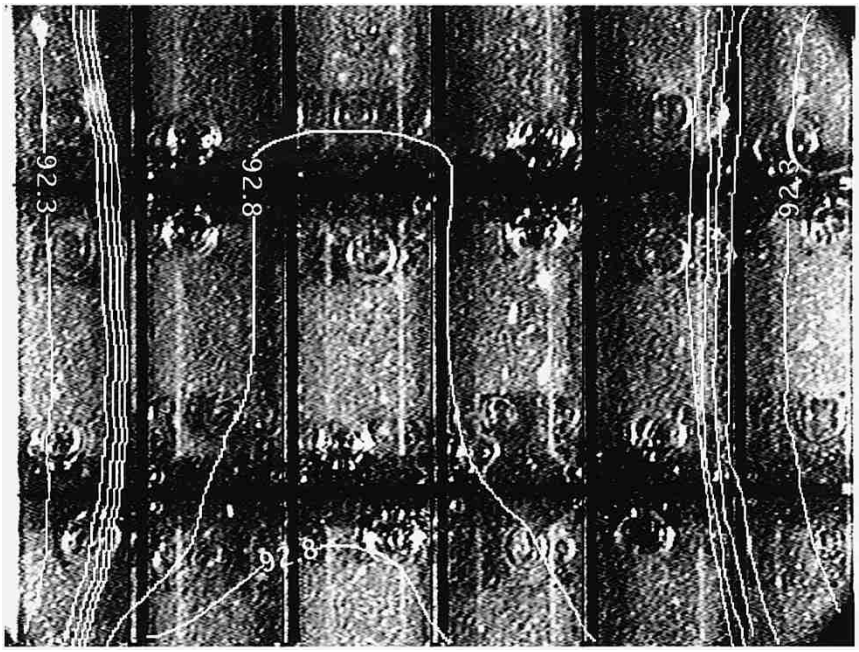

(a)

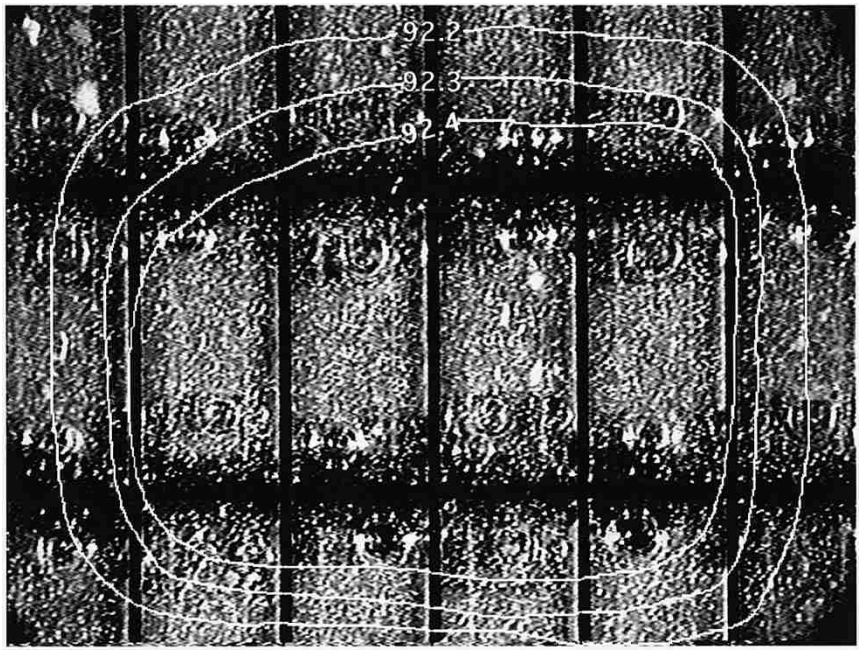

(b)

Fig. 7. Temperature profiles of silicon arrays under different clamping configurations. (a) Large contact-area clamp and heater at 95.0°C. (b) Small contact-area clamp and heater at 93.9°C. The two configurations require different heater temperatures to keep the liquid in a similar temperature range.

B. Measurements of Intravessel Temperature Uniformity

Variations of temperature within vessels can affect the uniformity with which reactions reach completion for a given set of reagents and, therefore, influence the precision of the PCR process, as discussed in Section I. For all interface and clamp choices described in Section III-A, the temperature uniformity within vessels near the threshold temperature of 55°C appeared to be better than 0.3°C, as shown in Fig. 8(f)–(j). The uniformity near the threshold temperature of 95°C, in contrast, appears to be significantly affected by the clamping method. The larger clamping area with the thermally conductive pad results in intravessel nonuniformity as high as 0.6°C in the peripheral vessels that are closest to the clamp, as shown in Fig. 8(d). The small clamp with the same pad results in intravessel nonuniformity of less than 0.4°C, as shown in Fig. 8(e). These observations support the conclusion that the intravessel uniformity is best at the center of the array, while the outer vessels have some three-dimensional (3-D) nonuniformity because the clamp contacts the array at the top and sinks heat. This effect is much more pronounced for the case of the large contact area, since this causes more heat

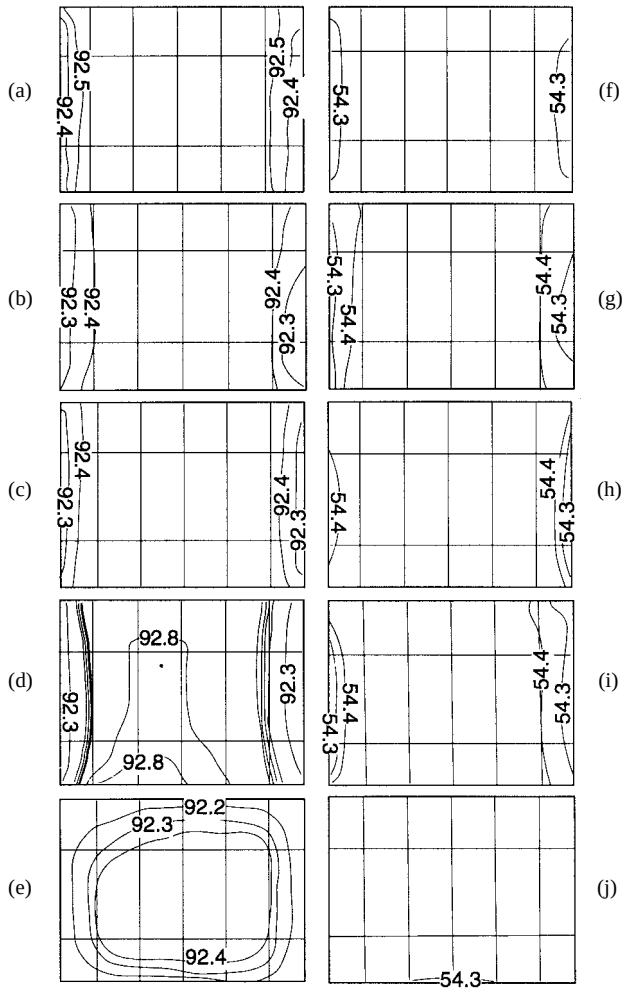

Fig. 8. Steady-state temperature field isotherms for different experiments. The captions denote the interface material and heater temperature. (a) No extra interface materials, 93.9°C. (b) Greased at lower left corner, 93.9°C. (c) Even greasing, 93.9°C. (d) Thermally conductive pad with large clamp, 95.0°C. (e) Thermally conductive pad with small clamp, 93.9°C. (f) No extra interface materials, 54.5°C. (g) Greased at lower left corner, 54.5°C. (h) Even greasing, 54.5°C. (i) Thermally conductive pad with large clamp, 54.5°C. (j) Thermally conductive pad with small clamp, 54.5°C.

to be drawn from the array and augments lateral temperature gradients.

It is useful to comment on the uniformity of temperature within the arrays during rapid changes in the die temperature, which is qualitatively observed during the ramping experiments and was predicted using the modeling at the end of Section II-F. According to heat diffusion theory, the time required for isothermal conditions to be achieved within a stationary region is comparable to L^2/α, where L is the characteristic dimension of the region and α is the thermal diffusivity. Using $L = 0.5$ mm and $\alpha = 1.5 \times 10^{-6}$ m^2/s for the liquid water region in a single vessel, it can be estimated that the temperature at the center of the vessel lags behind that at the walls by approximately 0.2 s, which is consistent with the experimental observations and with the more detailed modeling. This simple order of magnitude estimate is useful for determining the impact of the vessel dimensions on the thermal diffusion delays and, therefore, on the residence time required at the threshold temperature.

C. Time Constant

As discussed in Section II-F, the thermal time constant of the PCR system can be estimated by comparing the difference between the vessel array and heater temperatures at a given instant in time near the middle of a ramp in temperature. Fig. 9 plots the temperature difference as a linear function of the ramp rate and, therefore, has a slope equal to the time constant. The legend shows the calculated values for the time constant for the experimental cases. In all cases, the time constant measured using this method is less than 1 s. When using grease or no extra material at the interface, the time constant is always less than 0.25 s, while the thermally conductive pad increases the time constant to more than 0.75 s. These trials all use the large clamp. Regardless of the choice of interface material or clamp, the time constant is always less than 1 s, which is less than the time the temperature controller used in this experiment requires to stabilize at a target temperature.

The uncertainties in the calculated time constants shown in Fig. 9 can best be explained by the variability of the interface thermal resistance. Differences in clamping force, amount of grease, or the bonding of the adhesive tape could result in changes in the interface resistance which would show in the time constant. For the case of the small clamp [Fig. 9(b)], additional error may exist due to the difficulty in seating the clamp consistently, a problem which is very difficult to quantify into an error term. This additional error partially explains the appearance of nonlinearity to the curve. Beyond this possible source of apparent nonlinearity, the different components of the system can contribute to nonlinearity of response of the system. While all of the time constants for the heater, silicon, water, glass, and clamp have been lumped into one estimated time constant, in reality each component has its own unique time constant. Depending on the ramp rate, the effect of the time constant of each component on the calculated estimate will be different. However, using the water temperature provides the most conservative estimate of the time constant for the entire system.

IV. Conclusions

These thermometry experiments show that for the microfabricated vessel array in Fig. 2 and a variety of clamping methods and interface materials, the temperature variation among vessels is less than 1°C and the time constant is less than 1 s. The large-contact-area clamp drew a significant fraction of the power from the vessel array and resulted in a relatively large temperature nonuniformity and a larger time constant. The temperature nonuniformity was where the clamp contacted the array. A possible improvement to the clamping problem could be to add undercuts or corrugate the surface to reduce the contact area.

This work shows the promise of fluid thermometry in micromachined structures using immersed liquid crystals. Liquid crystal thermometry can be performed with relatively modest instrumentation and without costly one-time modifications to the micromachined structure. These are important benefits relative to thermometry using micromachined temperature sensors, such as electrical-resistance thermometers and thermocouple

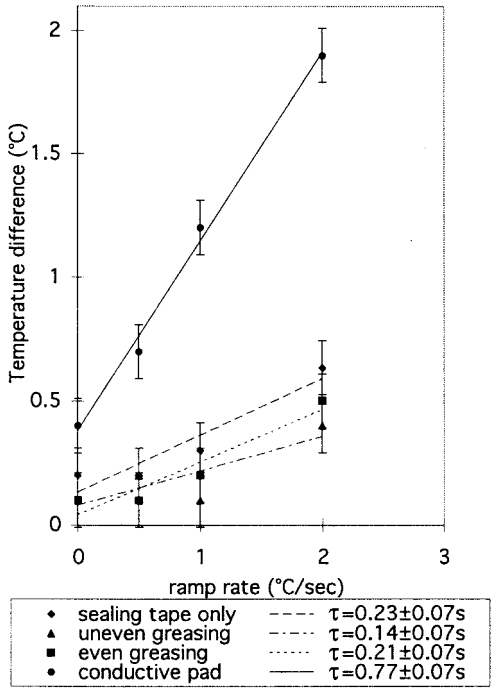

(a)

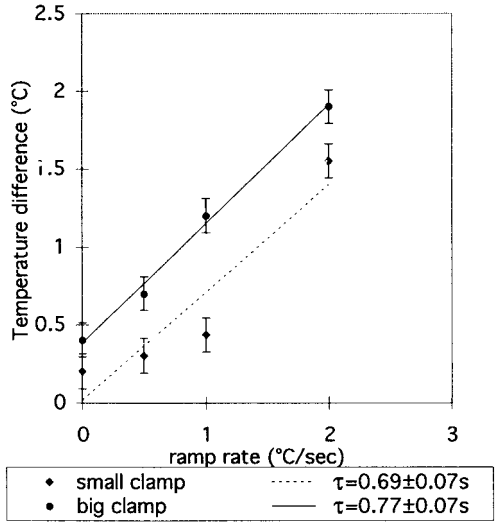

(b)

Fig. 9. Temperature differences for different ramp rates. (a) Large contact area clamp with different interface materials and (b) large versus small clamping format with thermally conductive pad as interfacial material.

junctions. Although liquid crystals offer a limited temperature bandwidth, the combination of crystals with different operational temperatures is an approach that is very well suited for devices operating at threshold temperatures, including the PCR devices studied here.

REFERENCES

[1] T. M. Woudenberg and J. Stevens, "Quantitative PCR by real-time detection," *Proc. SPIE*, vol. 2680, pp. 306–315, 1997.
[2] T. B. Taylor, E. S. Winn-Deen, E. Picozza, T. M. Woudenberg, and M. Albin, "Optimization of the performance of the polymerase chain reaction in silicon-based microstructures," *Nucleic Acids Res.*, vol. 25, pp. 3164–3168, 1997.
[3] M. A. Northrup, M. T. Ching, R. M. White, and R. T. Watson, "DNA amplification with a microfabricated reaction chamber," in *Transducers 1993*, pp. 924–926.
[4] M. A. Shoffner, J. Cheng, G. E. Hvichia, L. J. Kricka, and P. Wilding, "Chip PCR. I surface passivation of microfabricated silicon-glass chips for PCR," *Nucleic Acids Res.*, vol. 24, pp. 375–379, 1996.
[5] J. Cheng, M. A. Shoffner, G. E. Hvichia, L. J. Kricka, and P. Wilding, "Chip PCR II. Investigation of different PCR amplification systems in microfabricated silicon-glass chips," *Nucleic Acids Res.*, vol. 24, pp. 380–385, 1996.
[6] M. Parsley, *The Hallcrest Handbook of Thermochromic Liquid Crystal Technology*. Glenview, IL: Hallcrest, 1991.
[7] M. Parsley, "The use of thermochromic liquid crystals in research applications, thermal mapping and nondestructive testing," in *IEEE 7th Annu. Semiconductor Thermal Measurement and Management Symp.*, 1991, pp. 53–58.
[8] D. J. Farina, J. M. Hacker, R. J. Moffat, and J. K. Eaton, "Illuminant invariant calibration of thermochromic liquid crystals," *Visualization of Heat Transfer Processes*. New York: ASME, 1993, pp. 1–11.
[9] D. A. Coleman *et al.*, *Polymers and Liquid Crystals*. Cleveland, OH: Case Western Reserve Univ., 1996.
[10] M. J. Braun, M. Dzodzo, and S. B. Lattime, "Automatic computer based nonintrusive temperature measurements in laminar natural convection using TLC in enclosures with variable aspect ratio," *Experimental and Numerical Flow Visualization*. New York: ASME, 1993, pp. 111–119.
[11] D. Dabiri and M. Gharib, "Digital particle image thermometry. The method and implementation," *Experiments in Fluids*, vol. 11, pp. 77–86, 1991.
[12] F. P. Incropera and D. P. DeWitt, *Fundamentals of Heat and Mass Transfer*, 3rd ed. New York: Wiley, 1990, pp. 225–234.

Ajit M. Chaudhari received the B.S. degree in mechanical engineering and biological sciences in 1996 and the M.S. degree in mechanical engineering in 1997, both from Stanford University, Standford, CA. He is currently working towards the Ph.D. degree at Stanford University.

He is a National Defense Science and Engineering Graduate Fellow. At Stanford University, he specializes in gait analysis and mechatronics.

Timothy M. Woudenberg received the Ph.D. degree on the fluorescence spectroscopy of aromatic hydrocarbons seeded in a supersonic jet from Tufts University, Medford, MA.

He is a Senior Staff Engineer at PE Applied Biosystems, Foster City, CA, specializing in fluorescence detection systems. In his 11-year history at Perkin–Elmer, he breadboarded and was involved in the development of many PCR instruments and detection systems including the real-time monitoring of 5-in exonuclease work. He comes to Perkin–Elmer from the Chemistry Department, Tufts University.

Michael Albin received the Ph.D. degree from Penn State University, University Park.

He is Vice President of Science and Technology at PE Applied Biosystems, Foster City, CA. His main responsibility is technology assessment and business development. In his 8-year history at Applied Biosystems, he has been involved in the development of bioseparations, integration of micromachined structures, and sensors into bioinstrumentation.

Kenneth E. Goodson received the B.S., M.S., and Ph.D. degrees in mechanical engineering in 1989, 1991, and 1993, respectively, from the Massachusetts Institute of Technology, Cambridge. He also received the B.S. degree from Stanford University, Stanford, CA, in 1994.

He is currently an Assistant Professor and Frederick Emmons Terman Fellow with the Mechanical Engineering Department, Standford University, where he supervises eight doctoral candidates and one Post-Doctoral Associate who are investigating the thermal engineering of electronic microstructures. He spent 16 months with Daimler-Benz AG, Germany, working with the Materials Research Group on the thermal design of power circuits for vehicles. He is a Daimler-Benz CMG Research Advisor and a Texas Instruments FMA Program Advisor. In the Spring of 1995, he was a JSPS Visiting Professor at the Tokyo Institute of Technology, Tokyo, Japan. He is a coauthor of more than 28 archival journal articles and two book chapters.

Dr. Goodson is the recipient of the Louis Sudler Prize in Humanities, ONR Young Investigator Award, and NSF CAREER Award.